International Journal of Pressure Vessels and Piping 207 (2024) 105086

Contents lists available at ScienceDirect

International Journal of Pressure Vessels and Piping

journal homepage: www.elsevier.com/locate/ijpvp

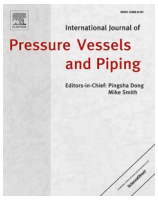

Probabilistic finite element-based reliability of corroded pipelines with interacting corrosion cluster defects

Abraham Mensah [a,b], Srinivas Sriramula [c,*]

[a] National Decommissioning Centre, School of Engineering, University of Aberdeen, Aberdeen, Scotland, UK
[b] Ghana National Gas Company (GNGC), Accra, Ghana
[c] School of Engineering, University of Aberdeen, Aberdeen, Scotland, UK

ARTICLE INFO

Keywords:
Pipeline burst pressure
Interacting corrosion cluster defects
Uncertainty quantification
Probabilistic finite elements
Sensitivity analyses
Surrogate model

ABSTRACT

The random distribution of pitting corrosion defects in pipelines normally leads to interacting cluster defects that behave noticeably different from single metal loss defects. Generally, the probabilistic approaches employ explicit burst pressure limit states for corroded pipelines subjected to only internal pressure. However, a significant level of conservatism is typically associated with the probabilistic assessments of corroded pipelines using the closed-form explicit limit state functions, which presents considerable challenges in maintenance planning and risk management. Therefore, this paper proposes a pathway for developing efficient performance functions for the assessment of interacting pipeline corrosion clustering defects using probabilistic finite element-based reliability method. This seven-stage framework combines multiple uncertainty representation schemes to evaluate the probability of failure. The impact of the critical design variables such as the elastic and plastic material properties, corrosion features, and interacting cluster defect characterisations are identified to guide the burst pressure design, operations and maintenance optimisation. The employed surrogate-based active learning reliability approach yielded an efficient probability estimate at a lesser computational cost than the simulation-based reliability methods. The proposed framework reduces the conservatism and computational cost related with explicit burst pressure limit state functions for corroded pipelines and offers informed decision-making on risk and maintenance management.

1. Introduction

The geometric, material characterisation and pressure loading parameters of corroded pipelines with interacting defect features exhibit intrinsic uncertainties due to manufacturing and operational processes, random distribution of pitting metal loss defects, and defect measurement mechanisms. The structural reliability estimates of corroded pipelines accommodating these uncertainties assist in developing cost-effective risk and maintenance management plans throughout the service life of the pipeline [1]. The reliability estimates of corroded pipelines with non-interacting and interacting defect features have historically used closed-form solutions developed from laboratory burst pressure experiments coupled with numerical methods using the traditional reliability methods such as the first order reliability method and Monte Carlo simulation (MCS) [2–6]. Valor et al. [2] examined the reliability of pipelines using a Monte Carlo reliability framework with explicit limit state function utilizing different corrosion rate distributions to study the performance of these rates with synthetic and real field data. Also, Teixeira et al. [3] assessed the reliability of corroded pipelines by employing explicit limit state function derived from burst experiments and numerical methods coupled with first order reliability method. Similarly, Bhardwaj et al. [4] used first order reliability algorithms and MCS techniques with explicit limit state function to evaluate the reliability of thick, highly corroded pipes under internal pressure load. Furthermore, Bisaggio and Netto [5] developed the structural reliability of corroded pipelines using explicit Det Norske Veritas (DNV) limit state function to compute the probability of failure of corroded pipelines over the lifecycle. However, these approaches are usually computationally expensive and produce results with a high degree of conservatism, especially for corroded pipelines with interacting corrosion clustering defects because of the highly non-linear behaviour. In a recent review of reliability analysis of part-wall metal loss pipelines subjected to internal pressure loads by Amaya-Gómez et al. [7], the conservative nature of employing explicit burst pressure limit state

* Corresponding author.
E-mail addresses: a.mensah.21@abdn.ac.uk (A. Mensah), s.sriramula@abdn.ac.uk (S. Sriramula).

https://doi.org/10.1016/j.ijpvp.2023.105086
Received 26 April 2023; Received in revised form 23 October 2023; Accepted 30 October 2023
Available online 31 October 2023

functions for reliability calculations for corroded pipes was emphasised. Hoang et al. [8] also highlighted the possibility of coupling numerical models with MCS to perform reliability analysis but expressed concerns on the computational cost. Furthermore, Gong et al. [9] underscored the need for a more thorough reliability framework that considers pipelines with localised interacting corrosion cluster defects rather than just a unit defect. This is highly essential, as very limited research has focused on developing a unified approach to evaluate interacting pipeline corrosion cluster defects.

Therefore, this study proposes a multi-stage probabilistic finite element-reliability method (PFERM), developing relevant developed surrogate models to estimate the probability of failure of a corroded pipeline with interacting corrosion clustering defects. This framework combines validated numerical models with probabilistic uncertainty quantification to identify machine learning based surrogates for applying active learning reliability techniques. The proposed approach offers the much-needed advantage of providing reliability estimates for corroded pipelines with interacting corrosion cluster defects or complex failure systems where, in some circumstances, a closed-form limit state function is not available. This unique pathway addresses the identified gap in terms of efficiency and computational cost related to burst pressure linked reliability assessment.

The paper is structured as follows: Section 1.0 presents the justification for the proposed methodology to estimate the reliability of corroded pipelines with interacting metal loss defect features. The details of proposed reliability approximation approach are provided in Section 2.0. Section 3.0 provides the quantification of the material, geometric, and pressure loading uncertainties and the related statistical analysis. The deterministic and probabilistic numerical modelling is described in Section 4.0. The results and outcomes from the reliability analysis are described in Section 5.0. The key findings, recommendations and limitations of this study are summarised in Section 6.0.

2. Methodology for the probabilistic finite element-based reliability of corroded pipelines

The seven stages of the proposed probabilistic finite element-based reliability method as proposed in Fig. 1, comprise the sub-elements of the surrogate model-based reliability analyses, leading to the selection of robust PFERM approach for risk and maintenance management.

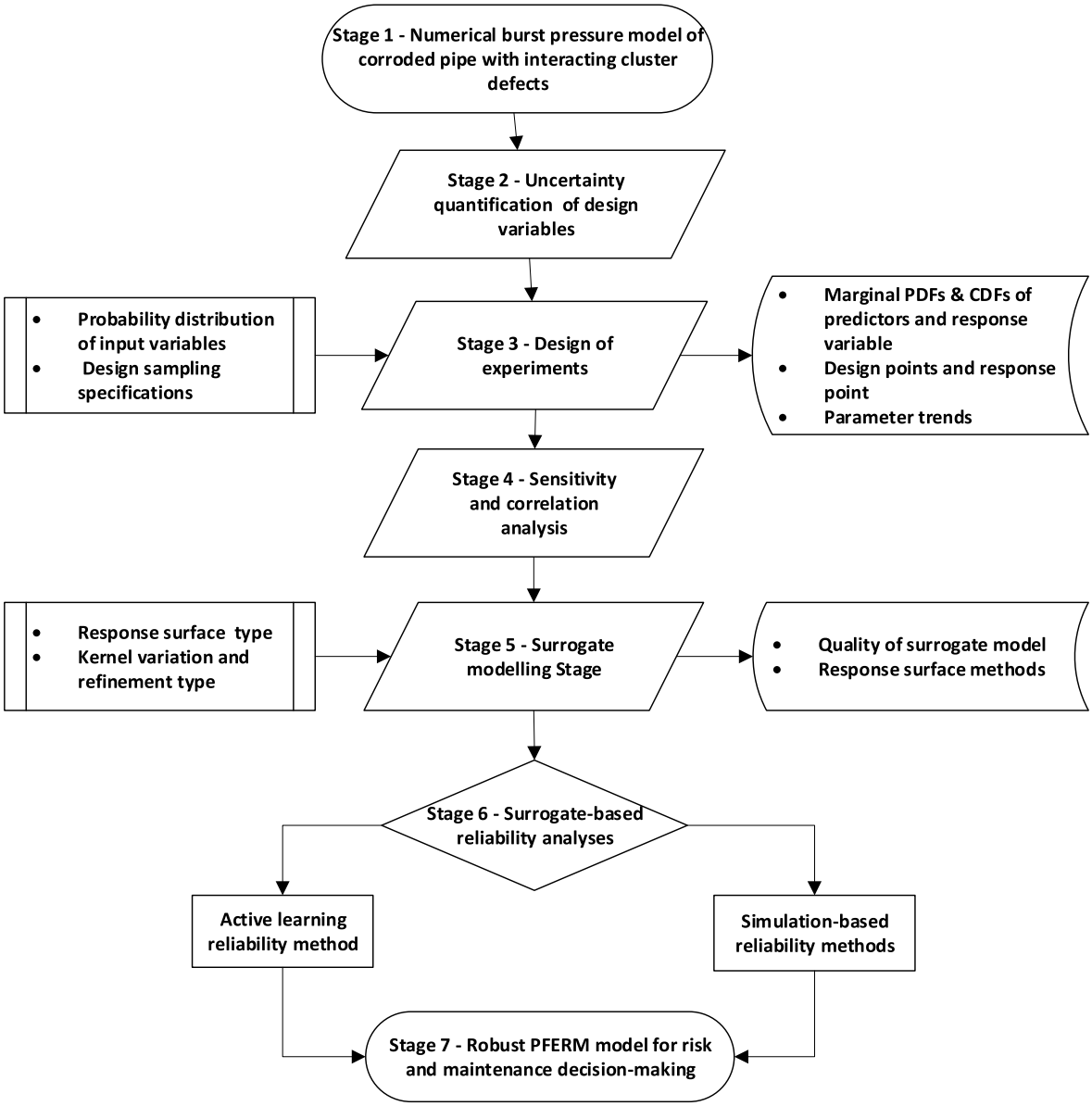

Fig. 1. Flowchart of Probabilistic Finite Element Reliability Method (PFERM) for evaluation of corroded pipelines.

A deterministic finite element-burst pressure model was developed in accordance with provisions from Ref. [10] utilizing the estimated mean values of the key material, geometric, and loading characterisations given in Table 1 of Section 3.0. A fully cylindrical meshed pipe with the required support systems to the relevant surfaces and nodes was modelled to prevent rigid body motion, plain strain settings, contraction, and expansion. This makes it possible to accurately capture the stress distribution of the unsymmetric corrosion clustering defects as displayed in Fig. 2. The true stress-plastic strain properties are included in the material definition to identify the failure pressure in the plastic deformation region of the pipe. The estimated burst pressure is validated with equivalent experiment results from Ref. [11] as presented in Section 4.1. The uncertainties in the material properties, the pipe and defect geometry characterisations, and the loading parameters are calculated from 25 sampling points in the burst pressure tests [11,12] under the Mixed Type Interaction (MTI) project, and are summarised in Table 1 of Section 3.0.

The initial step of the probabilistic numerical model is to combine the quantified uncertainty descriptors into the validated deterministic numerical model to generate the design and response sampling points, herein referred to as the Design of Experiments (DoE). The DoE approach adopts sampling, regression and interpolation techniques to derive design and response points that define the location of the critical design parameters of the burst model and the true burst pressure response of the model. The sampling techniques employed in this study include the central composite design (CCD), optimal space-filling design (OSFD) and the custom Kriging design.

The statistical dependency between the pipe material properties, internal pressure loading, pipe geometry and interacting corrosion cluster defect features are examined by using the Pearson, Kendall and Spearman correlation models as illustrated in Fig. 3. In this study, an input matrix of correlation coefficients between 11 variables in input vector X is computed. Then, the estimated matrix of the probability of occurrence, p-value of the null hypothesis of no correlation is tested against the alternative hypothesis of a nonzero correlation. If the computed *rho* is close to unity and the corresponding p-value is less than the significance level of 0.05, then the null hypothesis of no correlation is rejected, resulting in independent variables, which do not require a copula for the input model in the surrogate model. Otherwise, a copula definition will be required for the statistically dependent input variables. The sensitivities of the design variables in the DoE are determined using a sample-based sensitivity on the sampling points and the resulting predictors with significant impact on the burst pressure, which are then selected for the surrogate modelling stage. The surrogate model establishes a non-linear relationship between the design and response points, obviating the need for relatively computationally expensive numerical models. Regression and direct space interpolation methods such as Kriging, sector vector machine regression (SVR) and polynomial chaos-Kriging (PCK) approaches are applied to the design of experiments to generate the surrogate models with implicit limit states, which are used for reliability analyses of the corroded pipe. This is achieved by dividing the design of experiments by a ratio into two sets of data for training and validation purposes till the best combination yields a desirable level of performance.

The probability of failure of the corroded pipe due to the interacting corrosion cluster defects is estimated iteratively using a sample-based active reliability scripting on the developed PCK-surrogate model which contains the implicit limit state function. This is compared with the structural reliability estimates computed with simulation-based reliability approaches such as the Monte Carlo simulation, importance sampling and subset simulation. The robust PFERM approach for risk and maintenance management purposes is selected based on the efficiency of the reliability estimates and the cost of model simulation.

3. Uncertainty quantification of design variables based on published experimental observations

The suitable probability density distributions for the key variables are fitted using statistical approaches as summarised in Table 1. It is observed that they closely match the recommended distribution curves identified for reliability studies in Refs. [4,13]. The best probability density distribution fitting was confirmed by examining the relative frequency distributions from the experimental observations (Figs. 4–7), and also by performing Anderson-Darling goodness-of-fit tests by considering normal, lognormal, Weibull and Beta probability distributions to ensure that the probability value (p-value) for occurrence of such distribution exceeds the chosen significance level. The identified statistical descriptors and probability density functions for the random variables of the corroded pipeline system are given in Table 1.

The longitudinal and circumferential interacting corrosion defect spacing is the projected absolute minimum distance between the corrosion cluster defects in the longitudinal and hoop direction of the pipe, respectively. The effective defect cluster length and width is the projected total coverage length and width of a group of interacting corrosion defects in the longitudinal and hoop direction of a pipeline, respectively. The effective corrosion defect depth is the arithmetic mean of a group of interacting corrosion defects in a corroded pipeline. The histograms and probability plot shown in Figs. 4–7 showcase the variability of the design variables against the relative frequency or estimated cumulative probability respectively, from which the best distribution fit is identified for the probabilistic numerical modelling stage. The distributions for the quantified uncertainties relating to the material, geometric, and metal loss defect parameters are displayed in Figs. 4–7. The outliers in the distribution due to the selected fitting distribution curve were identified and considered appropriately in the DoE stage to capture the variability in the design variables. The material properties displayed in Fig. 4 show the relative frequencies based on the observed sample size, and therefore normal, lognormal, and Weibull distributions were considered. The lognormal distribution was selected as the best probability density function for the tensile yield strength and ultimate tensile

Table 1
Statistical representation of random variables.

No.	Input variables	Units	Mean	Standard deviation	Scale	Shape or Exponent	Location	Selected distribution
1	Tensile Yield Strength (SMYS)	MPa	624.480	32.970	0.053	–	6.436	Lognormal
2	Tensile Ultimate Strength (UTS)	MPa	732.000	28.520	0.039	–	6.595	Lognormal
3	Pressure Magnitude (*P*)	MPa	25.000	0.559	–	2	–	Beta
4	Minimum defect depth (*dmin*)	mm	3.770	2.060	4.199	1.914	–	Weibull
5	maximum defect depth (*dc*)	mm	4.790	1.544	5.452	3.689	–	Weibull
6	Outer Diameter of pipe (*D*)	mm	458.600	0.293	*	–	*	Normal
7	Pipe wall thickness (*t*)	mm	7.980	0.071	*	–	*	Normal
8	Effective defect cluster width (*Wc*)	mm	129.420	6.471	136.334	10.168	–	Weibull
9	Effective defect cluster length (*Lc*)	mm	210.000	10.500	221.921	9.632	–	Weibull
10	longitudinal interacting corrosion spacing (*SL*)	mm	30.000	1.500	31.508	9.757	–	Weibull
11	Circumferential interacting corrosion spacing (*Sc*)	mm	21.080	1.054	22.340	10.330	–	Weibull

Note: *-The location and scale for a normal distribution curve is the same as the mean and standard deviation, respectively.

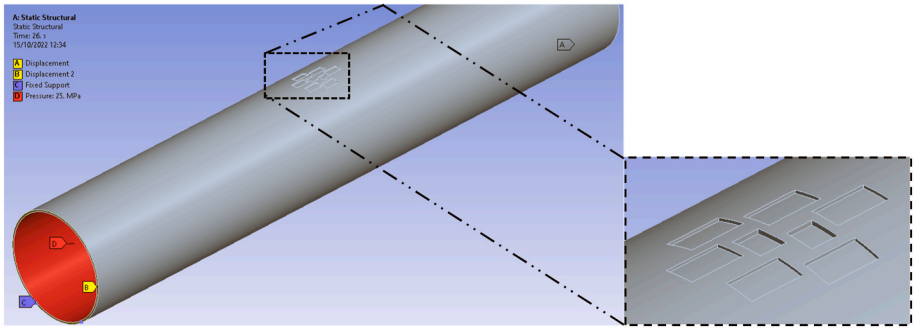

Fig. 2. Model configuration, boundary conditions and loading of pipeline interacting corrosion cluster defects.

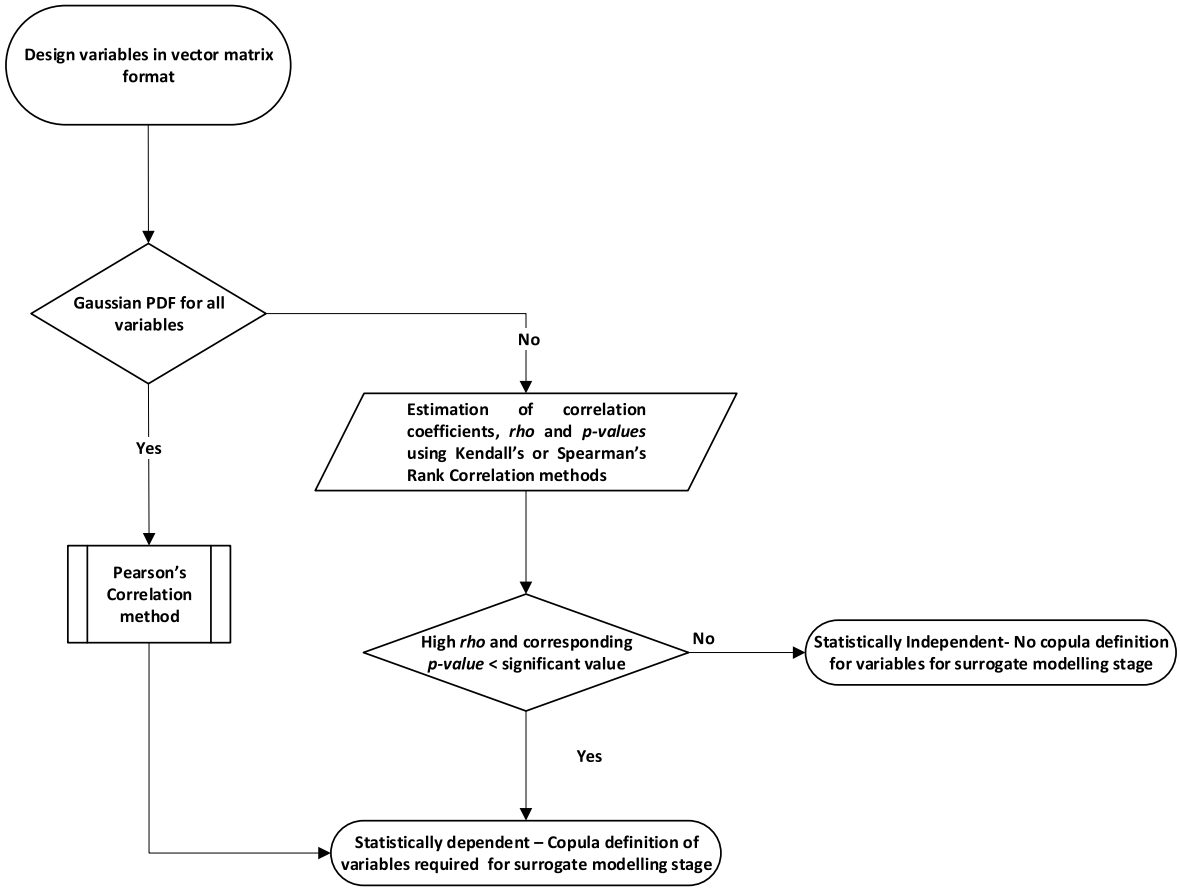

Fig. 3. Flowchart of Statistical dependence tests using Kendall and Spearman correlation methods.

strength as it yielded the highest p-value than the normal and Weibull distributions.

The normal distribution curve sufficiently described the variability of pipeline diameter and wall thickness parameters, exhibiting nearly symmetric characteristics as seen in Fig. 5.

The Beta distribution fits the internal pressure loading variables as seen in the probability plot with 95 % confidence level in Fig. 6.

The extreme value distribution type III, Weibull probability distribution was the best distribution fit for the available data of metal loss defect features (defect depth and length) and the interacting parameters in the longitudinal and circumferential direction of the pipe (effective corrosion cluster defect length and width, and the interacting corrosion cluster defect length in the longitudinal and hoop direction) as illustrated in Fig. 7. These skewed unsymmetric distributions exhibited significant deviations on one tail of the distribution.

The modelled continuous probability distribution curves showing the probability density function (PDF) and cumulative distribution function (CDF) for the described independent material, geometric and pressure characterisations in Table 1 are shown in Fig. 8. The PDF displays the probability description of the considered random variable, while the CDF provides the cumulative probability.

Pipe wall thickness (mm) Tensile Yield strength (MPa).

Effective corrosion cluster defect length (mm) Internal pressure (MPa).

4. Numerical modelling of corroded pipeline with interacting cluster defects

The process flowchart for the developed numerical modelling, as demonstrated in Fig. 9, comprises of a validated deterministic burst-pressure FEA model and a probabilistic finite element model. The key elements of the deterministic FEA model include model creation,

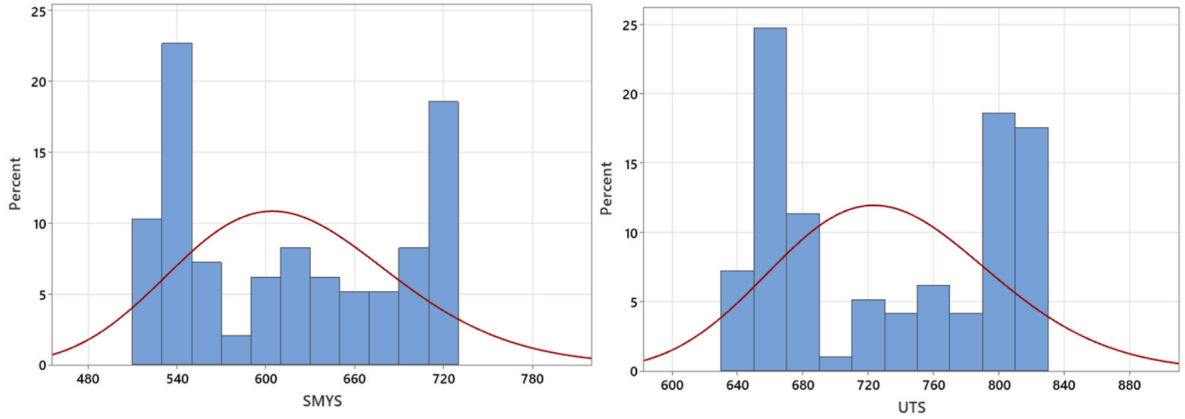

Fig. 4. Frequency distributions and lognormal probability fitting curves for the pipe material properties.

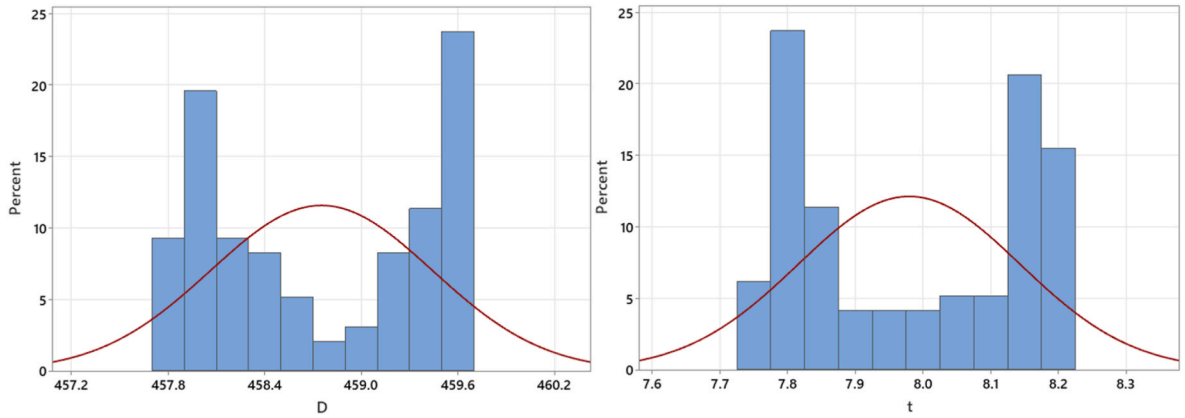

Fig. 5. Frequency distributions and lognormal probability fitting curves for pipe geometry.

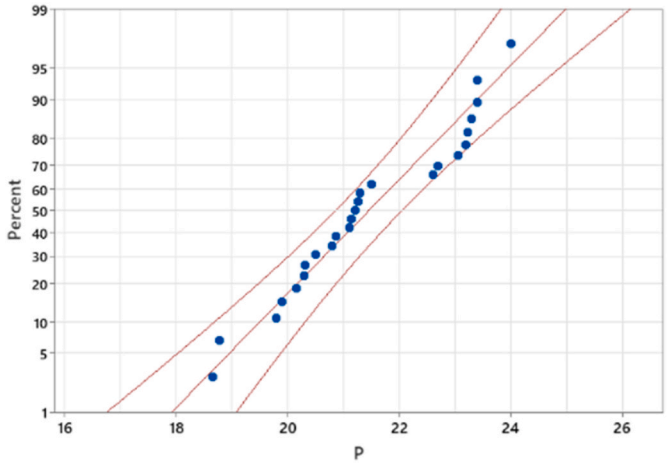

Fig. 6. Probability plot of pressure loadings.

material properties, and boundary conditions, including loading, meshing, and convergence analysis, failure criteria, and validation. The main components of the probabilistic numerical model from the validated deterministic FEA model include uncertainty quantification, experimental design using sampling techniques, and goodness of fit analysis to select the best model.

A static deterministic finite element model of corroded pipeline with external interacting corrosion cluster defects is produced by employing the same configuration (as shown in Fig. 2) from MTI [12] burst-pressure test sample number 22. A full-bore pipe is created due to the unsymmetrical nature of the defects in the cylindrical pipe by specifying the estimated pipe diameter and wall thickness mean - values from Table 1. To completely appreciate the stress distribution and deformations in the pipeline segment, this study utilizes a pipe length of six times the external diameter (*6D*), which meets the minimum requirement of *5D* as per BS 7910 [10]. The accurate arc lengths of the corroded surface with a depth length (*L*) and defect depth (*d*) are computed using an arc angle (∅) from the centre of the pipe in a plane as given in equation (1), to capture the exact volume of the corroded zones during the FEA model generation. A fillet with a radius of 0.05 mm is added to the intersections of the metal loss defects in the model geometry to minimise the stress concentration areas caused by abrupt ends or corners. The metal loss-interacting features are parameterized and set to the estimated mean - value estimates in Table 1. The arc angle (∅) is given by

$$\varnothing = \frac{\left(\frac{L}{2}\right)}{\left(\frac{D}{2} - d\right)} \cdot \frac{360^{\circ}}{2\pi} \tag{1}$$

The material properties of the pipe are created using the API 5L X80 grade carbon steel pipeline by specifying the elastic and plastic properties from De Andrade et al. [14]. The material's elastic properties comprise Young's modulus of elasticity, Poisson ratio, and the specified minimum yield strength (tensile yield strength), beyond which the pipeline experiences plastic (permanent) deformation. The pipe material's plastic properties are obtained by specifying the true stress-true strain property, including the ultimate tensile strength, which is the

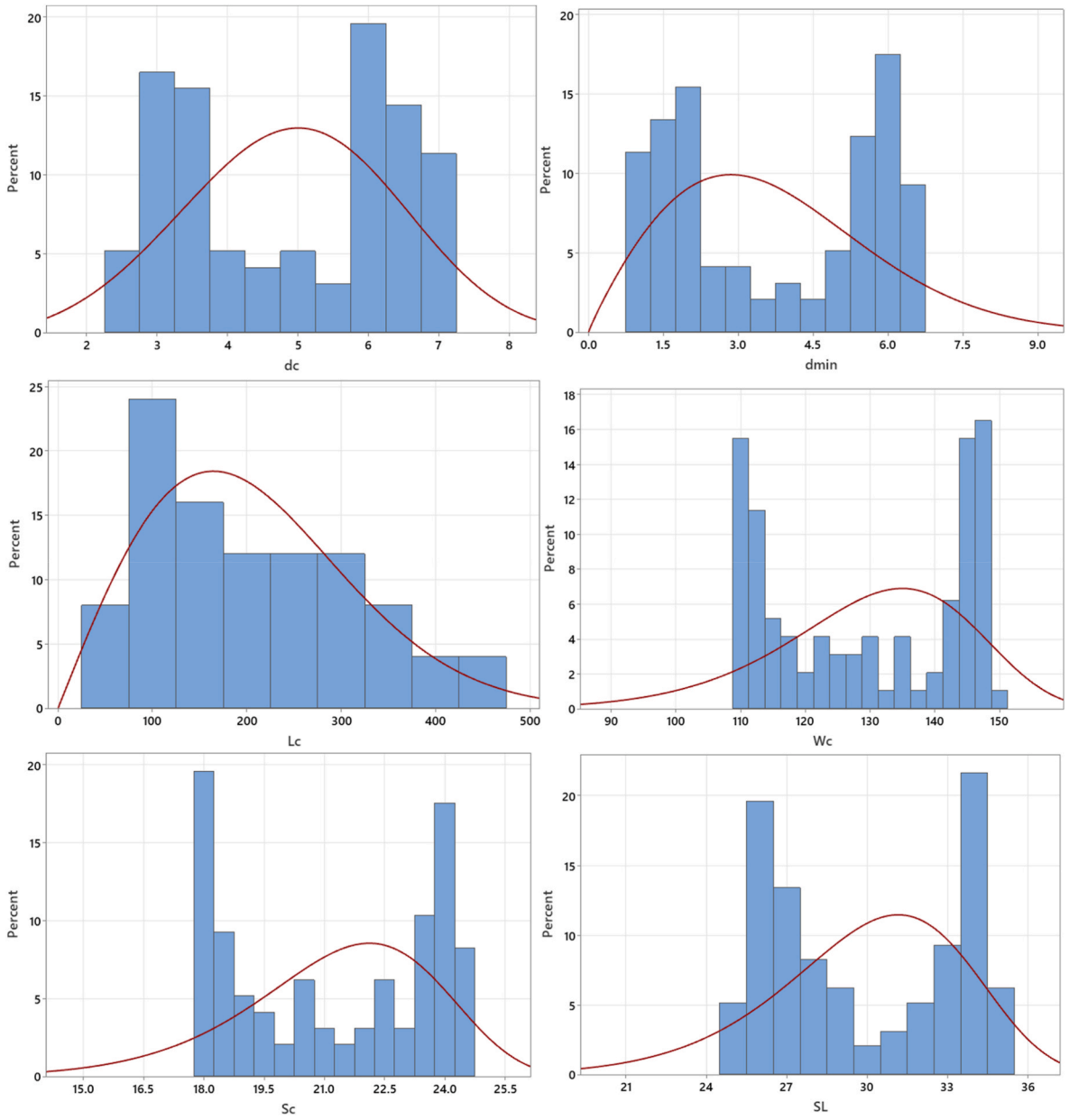

Fig. 7. Frequency distributions and Weibull probability fitting curves for corrosion defect features and interacting defect parameters.

maximum stress the pipe material can withstand in plastic deformation before it breaks. The model employs a 3-dimensional tetrahedral SOLID187 element (with 10 nodes exhibiting three degrees of freedom at each node) capable of fully displaying the irregular plasticity behaviour of the steel pipeline [15]. The pipe material properties are parameterized and set to the mean - value estimates from Table 1.

The faces of the two ends of the pipe (faces A and B) are restrained in the longitudinal direction of the pipe ($U_z = 0$) to prevent expansion and contraction in the longitudinal direction, as illustrated in Fig. 10. The two nodes at the extreme pipe end of the corroded pipe are fixed to prevent rigid body translation of the model in the three orthogonal directions of the pipe (thus, at nodes *C*, U_x=U_y=U_z=*0*). A mean - value internal pressure of 25 MPa is applied to the internal surface (Face D) of the pipe in a ramp function of 1 MPa per second to reveal the distinctive linear elastic section and non-linear plastic behaviour of the corroded pipeline.

The mesh density densities for the corroded region and the pipe body are set by specifying the element size along the length, width, and depth of each metal loss defect and across the pipe body, respectively, as shown in Fig. 11. For this study, the optimum element size is determined after convergence analysis as 1 mm along the defect length and width, as 0.5 mm along the defect depths, and as 50 mm across the pipe body, similar to studies in Refs. [16,17].

The failure pressure (burst pressure) is determined as the applied pressure at the instant when the equivalent von Mises stress through the pipe wall thickness of the corroded region reaches the ultimate tensile strength of the pipe material. The predicted failure pressure of the deterministic FEA model is validated with the MTI experimental bust pressure of test sample 22, as presented in Section 5.0. The validation of 25 samples using deterministic numerical methods with MTI experimental burst pressure is covered extensively in a recent publication by the authors [16].

The probabilistic model starts with the quantification of the uncertainties of material properties, geometric features of the pipe and corrosion defects, internal pressure loading, and interacting characterisations, as presented in Table 1. This is achieved by computing the

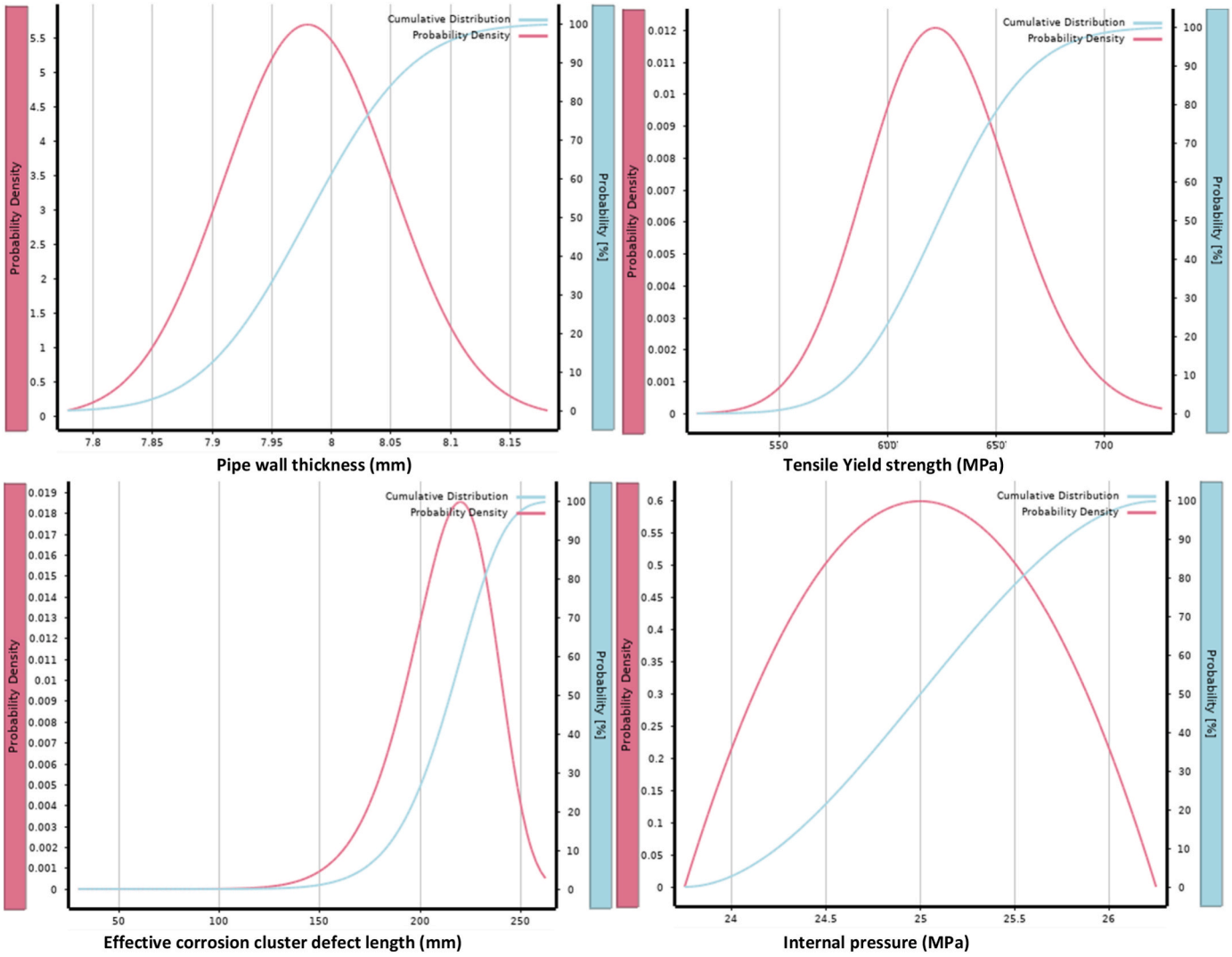

Fig. 8. Typical probability density distribution of uniform, Weibull and Beta characterisation.

statistical mean, standard deviation and the best-fit probability density function from the sampling data for the considered feature, as described in detail in Section 3.0. The quantified uncertainties are incorporated into the validated deterministic FEA model by sampling techniques to produce the design of experiments. The central composite design, the optimal space-filling design, and the Kriging design were the sampling methods used in the present investigation. The produced design of experiments generates the specified number of cases required. In this study, 100-number scenarios of different combinations of design variables are specified to derive a 100-number numerical burst pressure model response. The distribution fitting with the associated uncertainty can be estimated, but it is ignored in the reliability analysis stage, as determined by the sensitivity analysis in Section 5.3. The quality of the probabilistic FEA model is determined by the goodness of fit (coefficient of determination, root mean square error, and absolute maximum relative error) of the sampling method, sensitivity analysis, and trends of the predicted burst pressure, as presented in Section 5.0.

5. Application of the probabilistic finite element-based reliability method

The outcomes of the proposed PFERM approach are presented in this section. The key findings of the validated deterministic numerical modelling, surrogate model development, and reliability evaluation of the robust PFERM in terms of efficiency and computational cost are presented. The uncertainty quantification of the design variables is described in Section 3.0.

5.1. Validated deterministic numerical method

The predicted failure pressure from the developed deterministic numerical model of corroded pipelines with interacting metal loss clustering defects (explained in Section 2.0) is validated with the results from the MTI experiment [11] as highlighted in Table 2. The numerical model deviates from the test results by approximately 1 %, showing that the finite element burst model is acceptable. A validation of the 25 MTI samples using numerical method is given in a recent publication by the authors [16].

The probabilistic modelling aspect is initiated by adding the probabilistic descriptors of critical design variables from Table 1 to the parameterized and validated mean - value deterministic model and running the design of experiments to derive the sampling design and response points.

5.2. Validation of design of experiments from the probabilistic numerical model

The probabilistic numerical model of the corroded pipeline

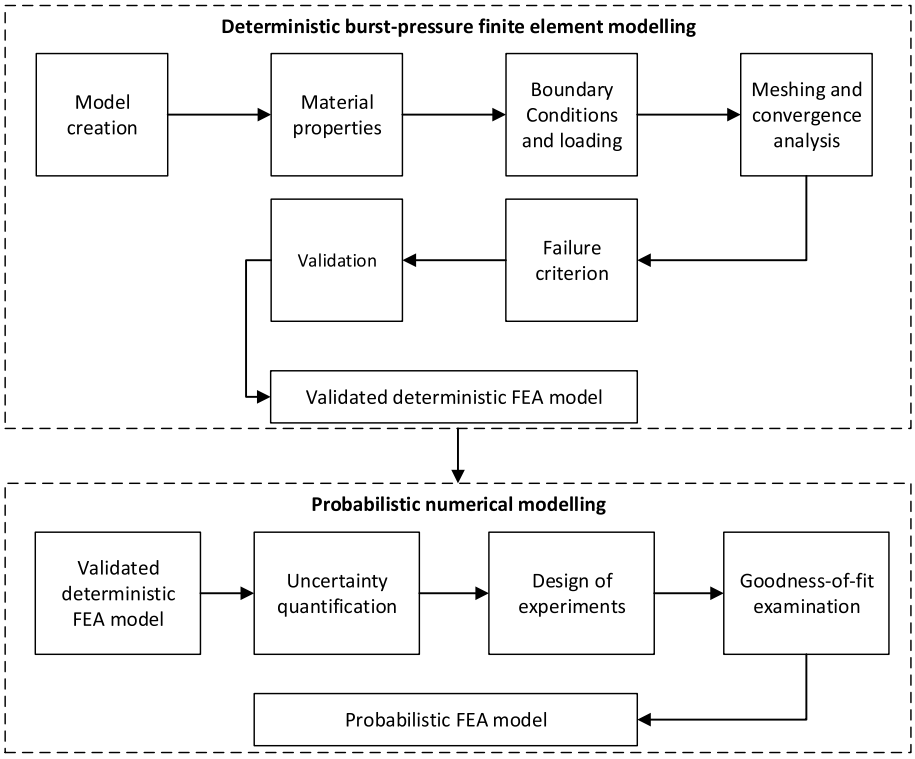

Fig. 9. Schematic of numerical modelling process.

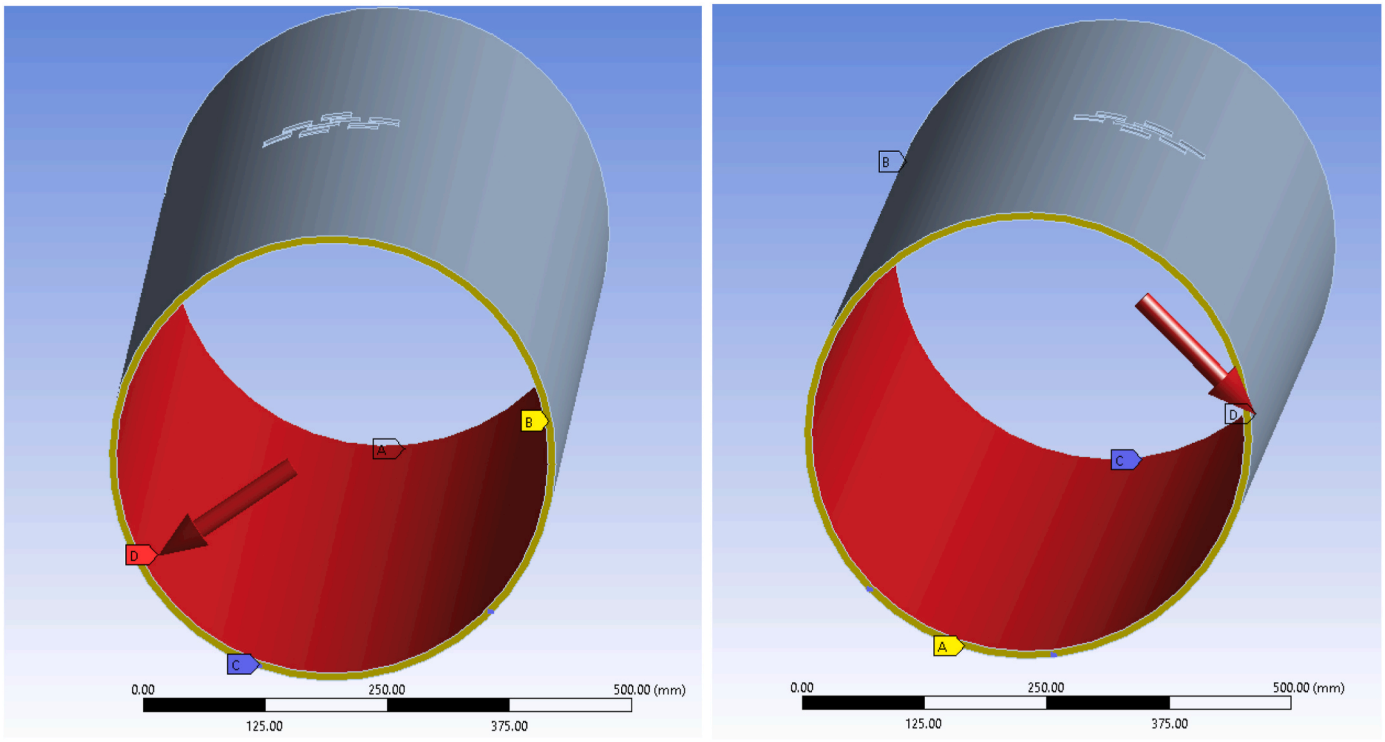

Fig. 10. Boundary conditions and internal pressure loading.

employed the central composite design (CCD), optimal space-filling design (OSFD) and the custom Kriging design sampling techniques to generate the design variable points and the failure stress response points in the DoE. The Kriging sampling design provided the best design space coverage and response surface fit by yielding a better coefficient of determination and error estimates in terms of Root mean square error and relative maximum absolute error than that of the CCD and OSFD, as displayed in Fig. 12. The custom Kriging approach has a comparative benefit over the fractional factorial design using CCD and OSFD in that it allows for the specification of the number of sampling points and offers a better response fit. The OSFD produces a response surface fit by uniform space distribution of the design points from fewer sampling points.

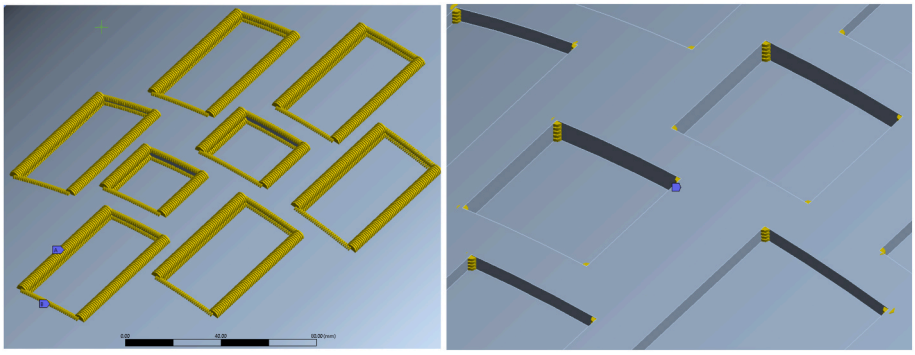

Fig. 11. Meshing of metal loss defects.

Table 2
Validation of deterministic model.

Test Sample	Predicted failure pressure from numerical model (MPa)	Experimental failure Pressure (MPa) [11]	Deviation (%)
22	20.500	20.300	0.985

However, this usually results in poor response prediction quality. The central composite design focuses on the parameter settings in the design region parameters to capture trends in the system but fails to capture the extreme ends of the design space [18].

The failure pressure of a corroded pipe depends on the pipe material properties (ultimate tensile strength), the pipe geometry (in terms of the pipe wall thickness and diameter) and the defect geometry based on the DNV [6] formulations in Equations (2) and (3).

$$P_f = UTS \times \left(\frac{2t}{D-t}\right) \times \frac{\left(1-\left(\frac{d_c^g}{t}\right)\right)}{\left(1-\left(\frac{d_c^g}{t}\right)\times\frac{1}{M_c^g}\right)} \tag{2}$$

where UTS is the ultimate tensile strength, t is the pipeline wall thickness, D is the outer diameter, d_c^g is the effective corrosion cluster depth, and M_c^g is the bulging factor. The Folias factor, M is defined in Equation (3).

$$M_c^g = \sqrt{1+0.31\left(\frac{L_C}{\sqrt[2]{Dt}}\right)^2} \tag{3}$$

Therefore, the failure stress of corroded pipe subjected to internal pressure, can be related to the failure pressure, as given in Equation (4).

$$\sigma_f = UTS \times \frac{\left(1-\left(\frac{d_c^g}{t}\right)\right)}{\left(1-\left(\frac{d_c^g}{t}\right)\times\frac{1}{M_c^g}\right)} \tag{4}$$

The sampling matrix comprising the design and response points is used for the sensitivity analyses to validate the influence of the design parameters on the true model response, as depicted in Section 5.3. Additionally, the trends in the design and response points in the DoE are described in this section to validate the probabilistic finite element model. The trend of the critical design variables of the corroded pipeline, such as the material properties, pipe and defect features, and interacting defect characteristics, is evaluated from the numerical model to highlight the behaviour of the corroded pipeline in relation to the predicted burst pressure.

It is observed in Fig. 13 that the predicted burst pressure from the probabilistic FEA model depends more heavily on the ultimate tensile strength (UTS) of the pipe material than the yield strength (SMYS)

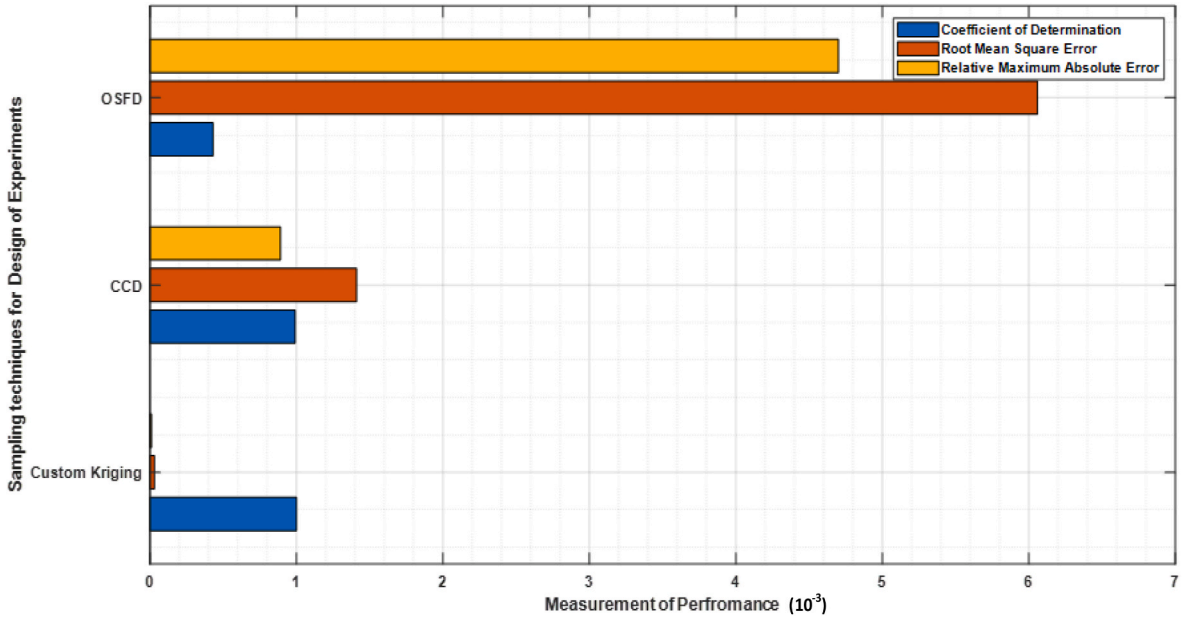

Fig. 12. Performance of the design of experiments sampling techniques.

property. The burst pressure of the corroded pipe increases noticeably with a rise in the UTS. For example, an increase in the pipe material UTS from 647.68 MPa to 826.09 MPa gives rise to a pipeline burst pressure of 22.17 MPa from 19.86 MPa, as shown in Fig. 13. The pipeline burst pressure marginally increases with an increase in SMYS, moving from 20.31 MPa to 20.60 MPa with a change of 529.37 MPa–734.69 MPa in the pipe's SMYS. From Fig. 13, it is worth noting that the mean - value estimates of the pipe's UTS and SMYS (732 MPa and 624.48 MPa, respectively) will lead to the predicted pipeline failure pressure of the validated deterministic FEA model, which is 20.5 MPa. The variability of the pipeline wall thickness and the effective corrosion cluster defect depth (*dc*) with respect to the predicted pipeline burst pressure is demonstrated in Fig. 14.

It is observed that the pipeline burst pressure increases significantly with an increase in the pipe wall thickness, while the burst capacity of the pipeline decreases with increasing effective metal loss cluster defect depth. This supports the DNV formulation in Equation (2). For example, in Fig. 14, the pipeline burst capacity increases from 19.80 MPa to 22.05 MPa, with a corresponding rise in pipe wall thickness from 7.76 mm to 8.20 mm. Notably, from Fig. 14, the mean - value estimates of the pipe's wall thickness and the effective corrosion cluster defect depth (thus 7.98 mm and 4.76 mm, respectively) lead to the predicted pipeline burst pressure of the validated deterministic numerical model, which is 20.5 MPa (from Table 2).

The trendline of the effective corrosion defect length and width with respect to the pipeline burst pressure capacity is presented in Fig. 15. It is generally noted that a decrease in the effective corrosion defect length and width leads to an increase in pipeline burst pressure capacity. However, a change in the effective corrosion defect length gives rise to a greater impact on the burst pressure than that of the width since it is perpendicular to the hoop direction of the corroded pipeline. For example, a noticeable decline in the pipeline burst pressure from 20.68 MPa to 19.94 MPa is observed when the effective corrosion defect length changes from 125.11 mm to 264.56 mm, while that of the width reduces linearly from 20.81 MPa to 20.29 MPa when the effective corrosion defect length changes from 83.91 mm to 158.59 mm (as shown in Fig. 15). Similarly, the mean - value estimates coincide with the burst pressure capacity of the validated deterministic FEA model.

Fig. 16 shows the marginal impact of the extreme value distributions of longitudinal and circumferential interacting corrosion defect spacing features on the pipeline burst pressure. Generally, the pipeline burst pressure capacity decreases marginally with increasing longitudinal and circumferential interacting corrosion defect spacing. Furthermore, it is observed that the interacting corrosion defect spacing in the hoop direction affects the pipeline burst pressure capacity more than the longitudinal interacting corrosion defect spacing. Notably, as the width and length of the interacting corrosion defects increase, thereby increasing the defect coverage area, the pipeline burst pressure capacity reduces sharply.

Fig. 17 shows how the pipeline external diameter affects the pipeline burst pressure capacity. It is found that at a constant wall thickness, the burst pipeline pressure decreases marginally with a corresponding increase in pipeline diameter. Significantly, the mean - value estimates of the pipeline external diameter of 458.6 mm coincide with the burst pressure capacity of the validated deterministic FEA model.

5.3. Correlation, sensitivity studies and surrogate modelling

The statistical dependency test of the input parameters is undertaken to determine the best approach for sensitivity analyses and surrogate modelling. It is observed from Table 3 that, none of the significant estimated correlation coefficients have the corresponding probability of occurrence below the significance level of 0.05. Hence, this pipeline system is treated as statistically independent.

Sensitivity analyses based on the design of experiments matrix are performed to determine the impact of the predictors on the true model response and select the influential design variables for the surrogate modelling stage. The sensitivities based on the Cotter index of key variables such as the material properties and defect characteristics to the true burst pressure response are demonstrated in Fig. 18. The Cotter sensitivity approach allows the ranking of the input variables (irrespective of the dependency between them) to determine the importance of the variables in terms of the model response [15]. It is worth noting that the failure mode heavily depends on the ultimate tensile strength (*UTS*) of the pipe material than the yield strength (*SMYS*), highlighting that the corroded pipeline fails by plastic deformation. Also, the model response depends more on the maximum corrosion cluster defect depth (*dc*), the pipeline external diameter (*D*) and the wall thickness (*t*) than the minimum corrosion cluster defect depth (*dmin*). The effective cluster defect length (*Lc*) in the longitudinal direction of the interacting defect

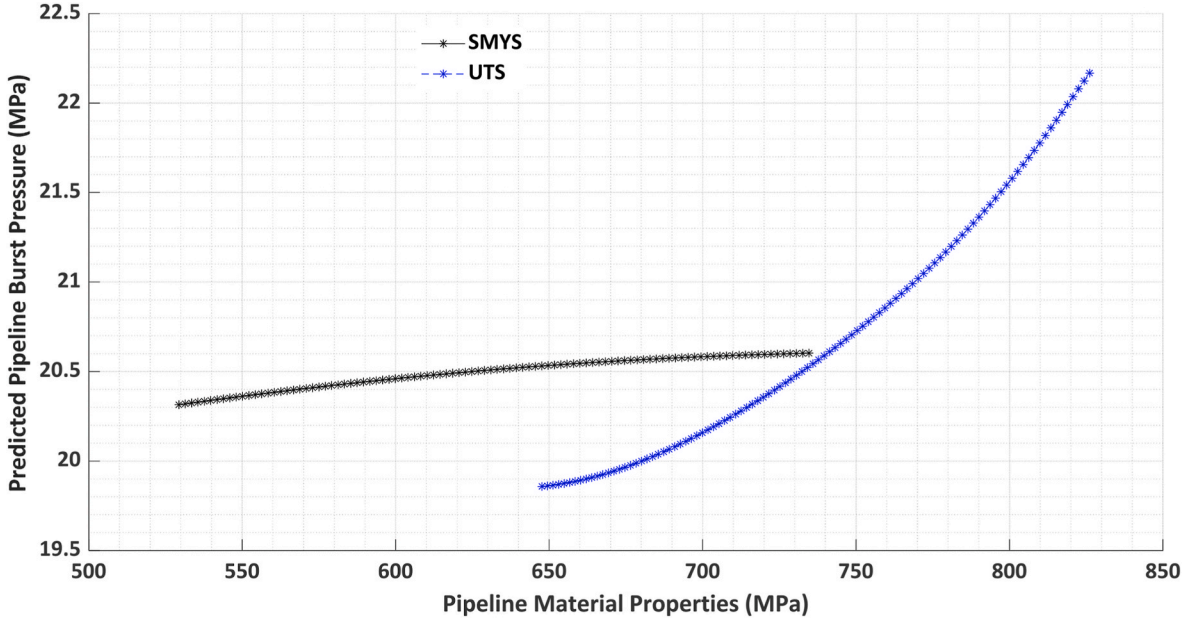

Fig. 13. Trendline of the material properties (UTS and SMYS) to pipeline burst pressure capacity.

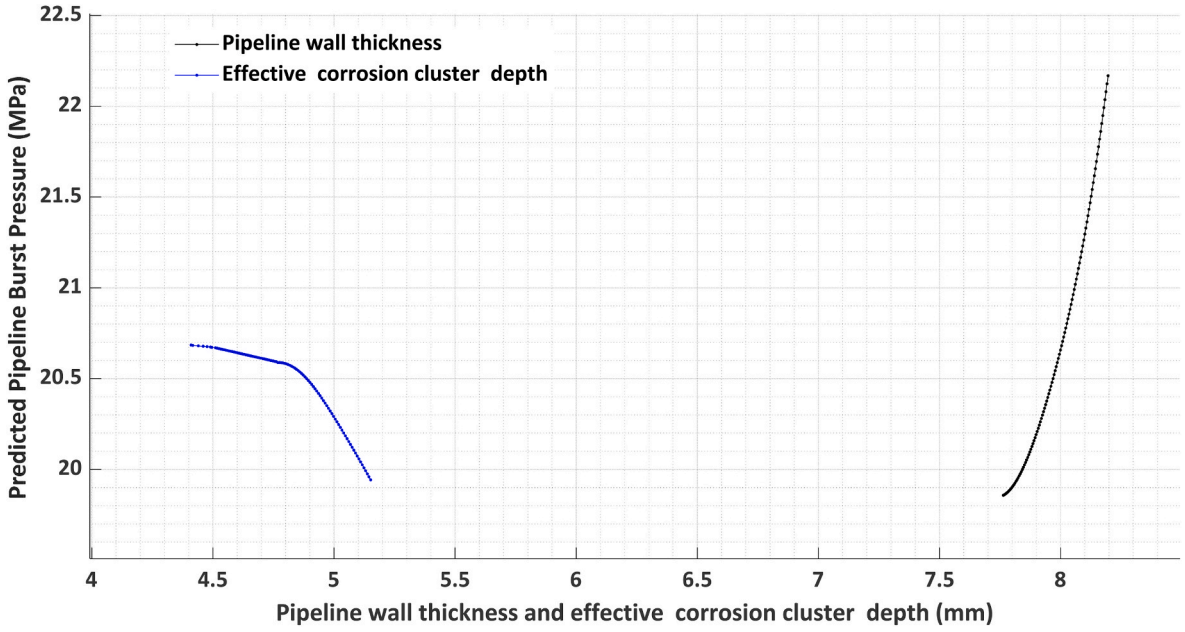

Fig. 14. Trendline of the pipe wall thickness and effective corrosion cluster defect depth to the pipeline burst pressure.

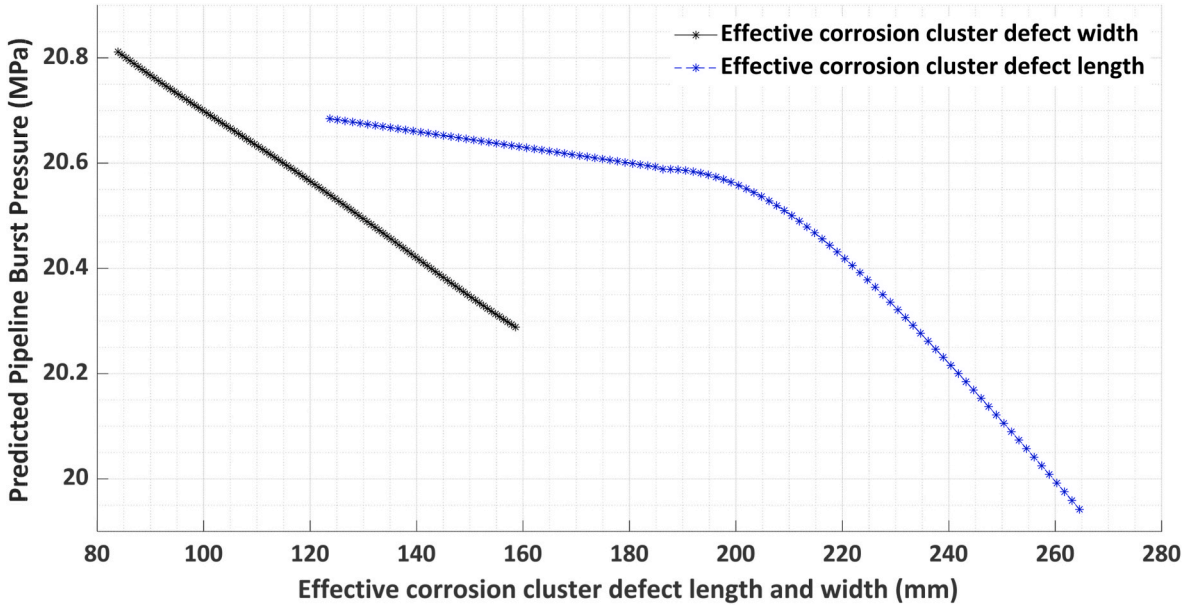

Fig. 15. Trendline of the effective corrosion cluster defect length and width to the pipeline burst pressure capacity.

colonies contributes most to the pipeline failure response. The influence from the effective corrosion cluster defect length (*Lc*) and longitudinal interacting corrosion defect spacing (*SL*) are greater than the influence from the effective corrosion cluster defect width (*Wc*) and circumferential corrosion cluster defect spacing (*Sc*), although the interacting parameters in the hoop direction cannot be ignored unlike propositions by Silva et al. [19]. For this study, the tensile yield strength, the internal pressure (*P*), minimum corrosion cluster defect depth and the effective corrosion cluster defect width are overlooked in generating the metamodels based on a Cotter index limit of 0.025.

The surrogate model was developed by applying regression and machine learning methods such as the Kriging, sector vector machine regression (SVR) and polynomial chaos-Kriging (PCK) to establish a nonlinear relationship between the screened design and response points. The predicted model by PCK yielded the least leave-one-out error from the true model response of 0.40×10^{-3}, better than the errors of 2.22×10^{-3} and 6.94×10^{-3} produced by polynomial Kriging and SVR, respectively as shown in Table 4. This could be because the PCK employs orthogonal polynomials which tend to capture the global behaviour in addition to the local interpolation of the design space, unlike Kriging and SVR that employ interpolation and sequential minimal optimisation processes, respectively.

The metamodels with implicit limit states are developed using regression and machine learning methods such as the polynomial chaos-Kriging approach as it tends to capture the global behaviour in addition to the local interpolation of the design points better than polynomial Kriging and sector vector machine regression.

The spatial response surface fit generated by the polynomial chaos-Kriging provides the relationship between the spatial variability in the key design variables and the predicted model response as illustrated in

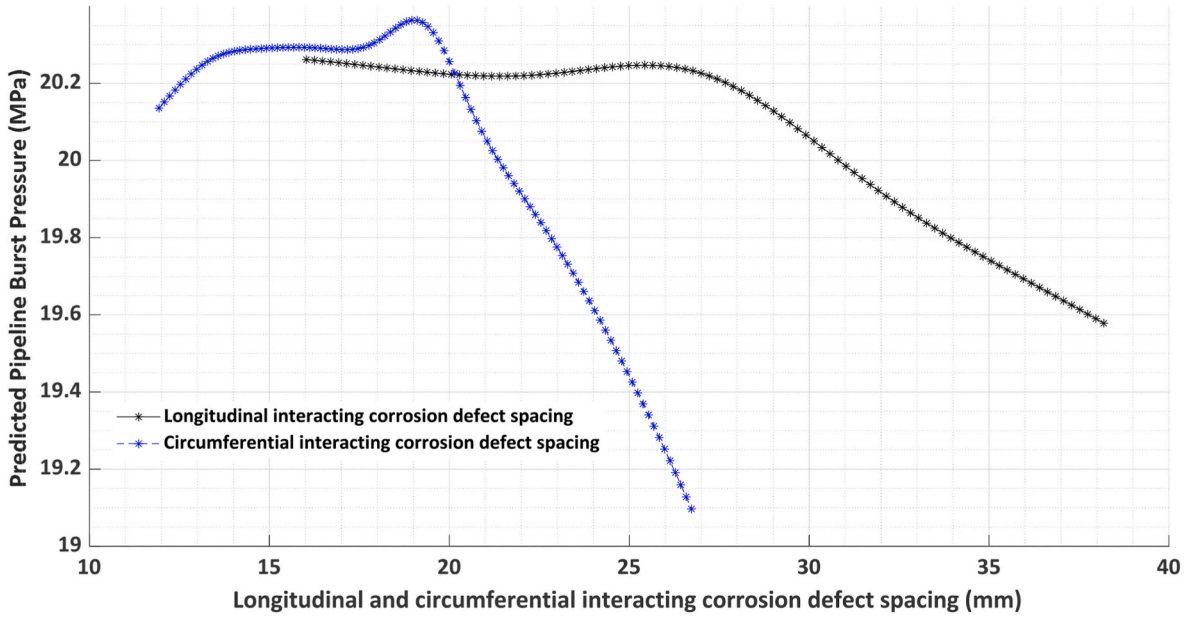

Fig. 16. Trendline of the longitudinal and circumferential interacting corrosion defect spacing to pipeline burst pressure.

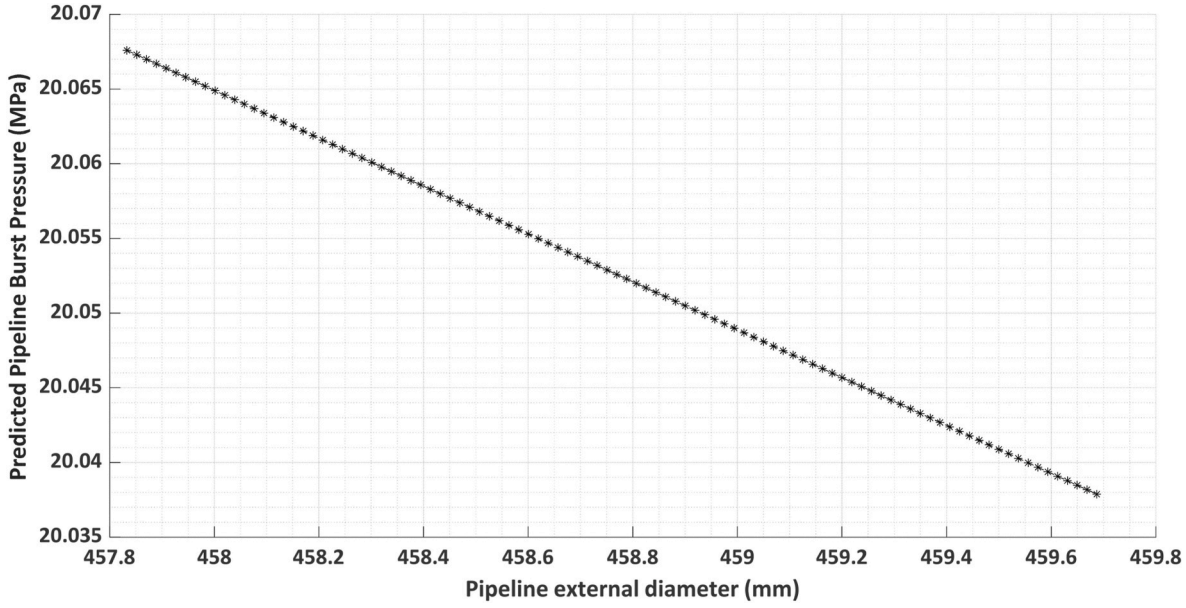

Fig. 17. Trendline of the pipe external diameter to pipeline burst pressure.

Fig. 19. It offers the opportunity to determine the model burst pressure failure response point within the spatial sampling space given any two design variables [20].

The generated cumulative distribution function (CDF) of the response variable from the design parameters, as demonstrated in Fig. 20 is essential to check that the probability of the failure stress at the corroded region of the pipe remains below a specified criterion. For example, the probability of attaining a failure stress of about 745 MPa and 752 MPa is 30 % and 90 % respectively.

5.4. Implicit limit state function-based reliability analysis

A surrogate-based active learning reliability approach was used to determine the probability of failure (Pf) of the corroded pipe, and the results are shown in Table 5 alongside the simulation-based reliability approaches.

The active learning reliability estimates were achieved by adding limit state function evaluations from the experimental design in the PCK-surrogate model until a convergence criterion for the P_f is reached. Based on the active learning reliability plot in Fig. 21, the estimated P_f is approximately 1.9789×10^{-7} when 122 model evaluations from the design sampling points in the PCK metamodel are added. The simulation terminated at the 122nd sample point when the minimal distance to the other experimental design points is beyond 10^{-2} of the minimum distance between the design points at the first iteration.

The performance of the employed surrogate model-based reliability method is compared with the simulation-based methods by considering the probability of failure estimation within a reliable confidence interval and the computational cost considering the number of model evaluations. From Table 5, Figs. 21 and 22, it is worth noting that the

Table 3
Typical correlation results using Kendall Tau's ranking method.

Estimated correlation coefficient, rho											
Variable	SMYS	UTS	P	dmin	dc	D	t	Wc	Lc	S_L	S_C
SMYS	1.0000	0.0481	0.0012	−0.0392	0.0024	−0.0032	0.0202	−0.0339	0.0315	0.0267	0.0436
UTS	0.0481	1.0000	−0.0238	0.0238	0.0089	−0.0057	0.0016	0.0040	−0.0533	−0.0436	−0.0291
P	0.0012	−0.0238	1.0000	−0.0683	−0.1018	−0.0978	−0.0154	0.0121	−0.0380	−0.0622	−0.0065
dmin	−0.0392	0.0238	−0.0683	1.0000	0.0739	0.0781	0.0315	0.0097	0.0097	−0.0525	−0.0097
dc	0.0024	0.0089	−0.1018	0.0739	1.0000	0.0852	0.0529	−0.0036	−0.0271	−0.0505	0.0352
D	−0.0032	−0.0057	−0.0978	0.0781	0.0852	1.0000	0.0505	0.0053	0.0028	−0.0392	0.0246
t	0.0202	0.0016	−0.0154	0.0315	0.0529	0.0505	1.0000	−0.0287	0.0028	−0.0012	0.0206
Wc	−0.0339	0.0040	0.0121	0.0097	−0.0036	0.0053	−0.0287	1.0000	0.0085	0.0198	−0.0909
Lc	0.0315	−0.0533	−0.0380	0.0097	−0.0271	0.0028	0.0028	0.0085	1.0000	0.0820	0.0537
S_L	0.0267	−0.0436	−0.0622	−0.0525	−0.0505	−0.0392	−0.0012	0.0198	0.0820	1.0000	−0.0198
S_C	0.0436	−0.0291	−0.0065	−0.0097	0.0352	0.0246	0.0206	−0.0909	0.0537	−0.0198	1.0000
Probability of occurrence, p-value											
Variable	***SMYS***	***UTS***	***P***	***dmin***	***dc***	***D***	***t***	***Wc***	***Lc***	S_L	S_C
SMYS	1.0000	0.4803	0.9881	0.5654	0.9739	0.9644	0.7681	0.6189	0.6444	0.6964	0.5220
UTS	0.4803	1.0000	0.7275	0.7275	0.8981	0.9359	0.9834	0.9549	0.4335	0.5220	0.6702
P	0.9881	0.7275	1.0000	0.3156	0.1341	0.1503	0.8233	0.8605	0.5776	0.3606	0.9264
dmin	0.5654	0.7275	0.3156	1.0000	0.1850	0.2640	0.6444	0.8887	0.8887	0.4405	0.8887
dc	0.9739	0.8981	0.1341	0.1850	1.0000	0.1800	0.4370	0.9596	0.6920	0.4584	0.6064
D	0.9644	0.9359	0.1503	0.2640	0.1800	1.0000	0.4584	0.9407	0.9691	0.5654	0.7186
t	0.7681	0.9834	0.8233	0.6444	0.4370	0.4584	1.0000	0.6745	0.9691	0.9881	0.7636
Wc	0.6189	0.9549	0.8605	0.8887	0.9596	0.9407	0.6745	1.0000	0.9028	0.7727	0.1812
Lc	0.6444	0.4335	0.5776	0.8887	0.6920	0.9691	0.9691	0.9028	1.0000	0.2278	0.4300
S_L	0.6964	0.5220	0.3606	0.4405	0.4584	0.5654	0.9881	0.7727	0.2278	1.0000	0.7727
S_C	0.5220	0.6702	0.9264	0.8887	0.6064	0.7186	0.7636	0.1812	0.4300	0.7727	1.0000

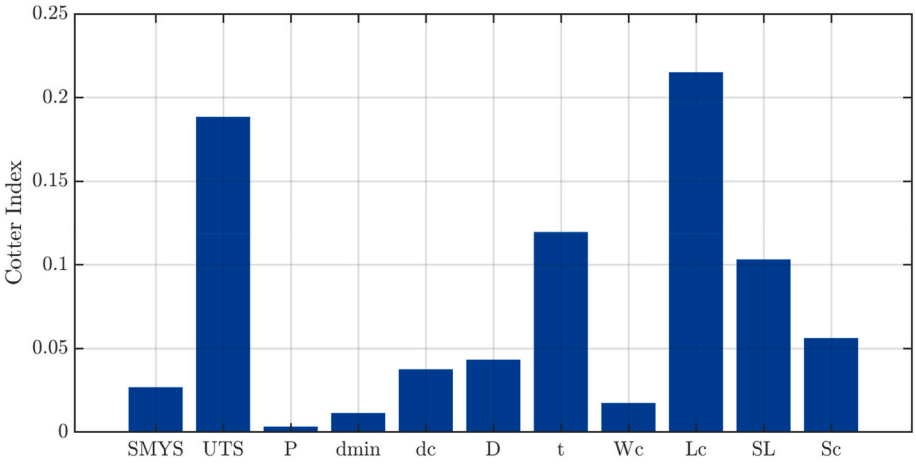

Fig. 18. Sensitivity of design variables using Cotter sensitivity method.

Table 4
Performance of surrogate modelling approaches.

Metamodel Method	Kriging	Polynomial Chaos-Kriging	Sector Vector Machine Regression
Leave-out-error ($\times 10^{-3}$)	2.22	0.40	6.94

probability of failure estimates by all the considered reliability methods is in the region of 10^{-7}. However, the active learning reliability method provides a reliable and narrow confidence interval for the probability of failure between 1.5473 $\times 10^{-7}$ to 2.4105 $\times 10^{-7}$ while a simulation method such as the importance sampling simulation yields a wider confidence interval between 9.5996 $\times 10^{-8}$ to 2.9600 $\times$ 10^{-7}. Additionally, the active learning reliability provides lower computational cost than the simulation-based methods by converging with 122 number of samples, N unlike the simulation-based reliability approach such as Monte Carlo simulation, importance sampling simulation and subset simulation that converged after 10^7 model evaluations, 10^7 model evaluations and 73000 model evaluations, respectively.

6. Conclusions

The probabilistic assessment of corroded pipelines using explicit limit state functions generally leads to conservative reliability estimates that significantly affect risk management and maintenance planning. Also, in many instances explicit representation of limit states is not possible. This study proposes an implicit limit state function approach to estimate the probability of failure of the corroded pipeline with interacting defect features by combining design of experiments generated from the probabilistic numerical model, surrogate models from design of experiments using machine learning techniques and reliability simulation on the surrogate models.

The following inferences were established from the probabilistic finite element-based reliability method (PFERM) for the assessment of the interacting corrosion cluster defects in the pipeline. To begin, the uncertainty in the material properties (tensile yield strength and tensile

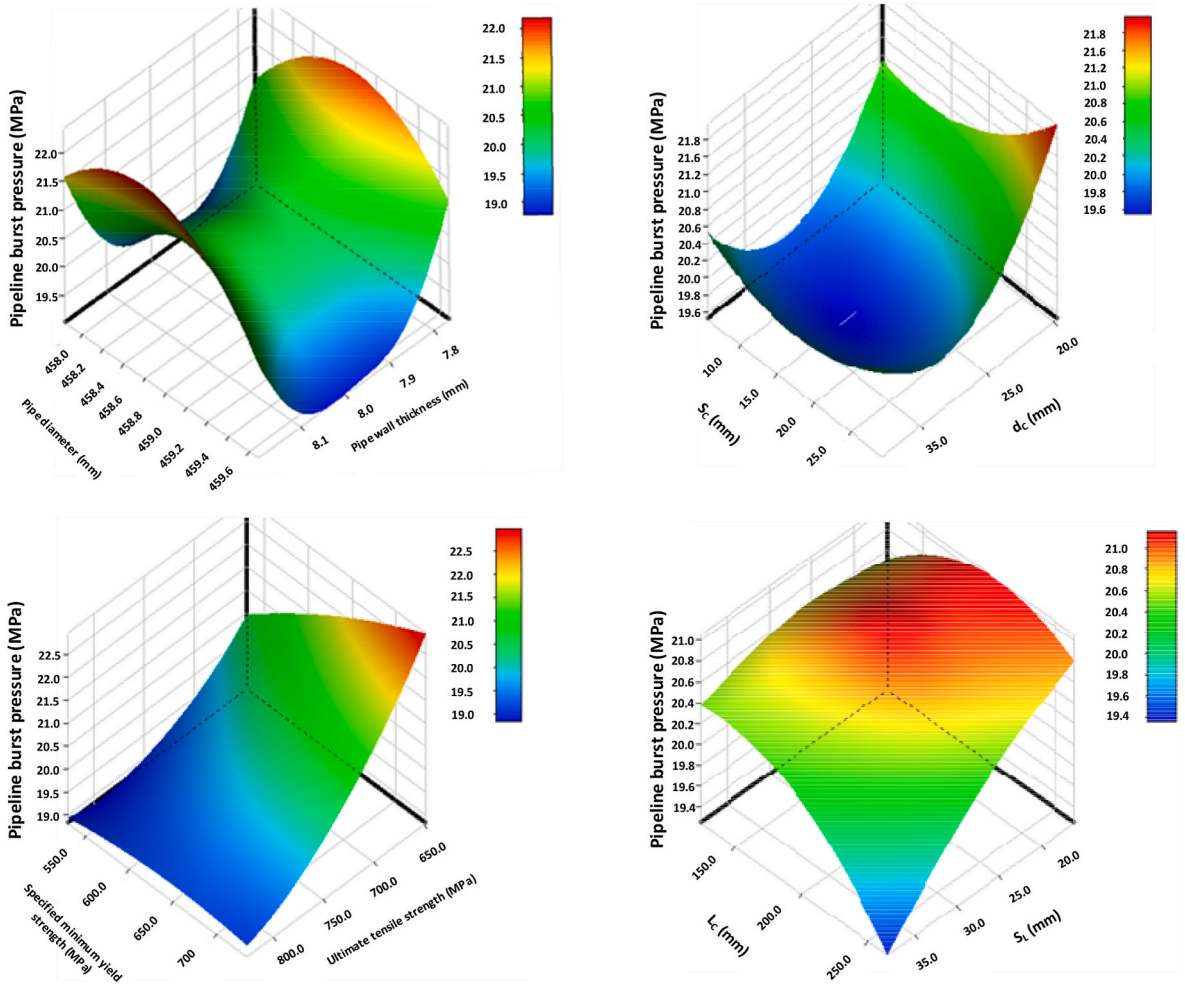

Fig. 19. Spatial variation of key material and geometric characterisations and the pipeline burst pressure.

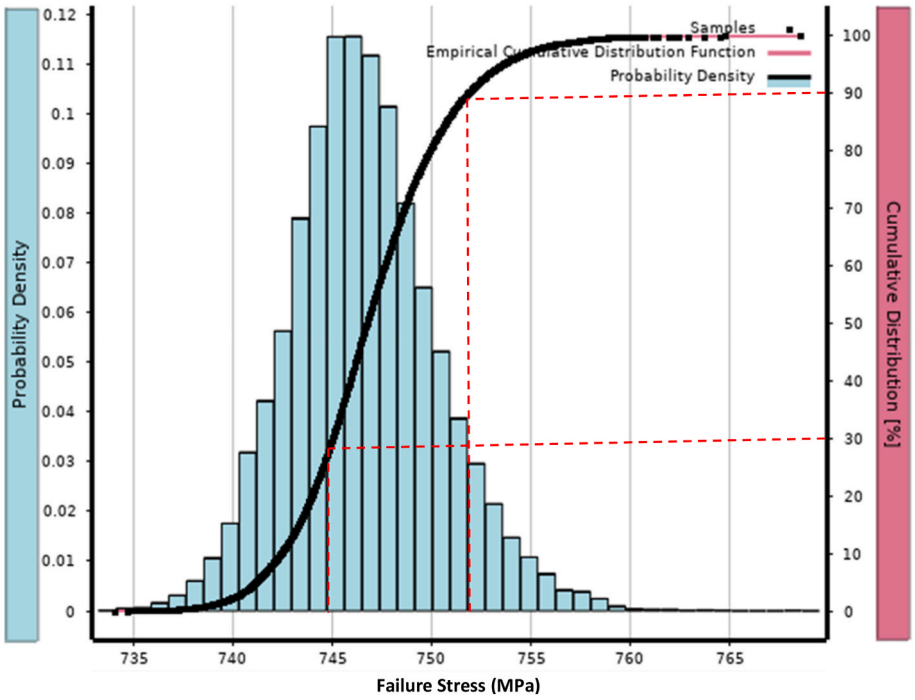

Fig. 20. Cumulative distribution function of the pipeline failure stress.

Table 5
Summary of reliability estimates of corroded pipeline.

No.	Reliability descriptors	Reliability Approach			
		Active Learning Reliability	Monte Carlo Simulation	Importance Sampling	Subset Simulation
1	Probability of failure (P_f)	1.9789 × 10^{-7}	1.0000 × 10^{-7}	1.0000 × 10^{-7}	1.6700 × 10^{-8}
2	Reliability Index (β)	5.0710	5.1993	5.1993	5.5226
3	Coefficient of Variation (*CoV*)	0.1113	1.0000	1.0000	0.1592
4	Model Evaluations	122.0000	10000000	10000030	73000
5	Confidence Interval for P_f (P_f*CI*)	[1.5473 × 10^{-7} 2.4105 × 10^{-7}]	[-9.5996 × 10^{-8} 2.9600 × 10^{-7}]	[-9.5996 × 10^{-8} 2.9600 × 10^{-7}]	1.1490 × 10^{-8} 2.1910 × 10^{-8}

ultimate strength), geometric characterisations (pipe diameter, wall thickness, interacting defect features) and internal pressure loading are quantified. The best distribution fits were examined by the Anderson-Darling test and probability plots, and it was observed that the normal, Weibull, and the Beta probability density distributions provided the best fit for the pipeline geometry (external diameter and wall thickness), metal loss features (maximum and minimum corrosion cluster defect depth, effective corrosion cluster defect length and width, and longitudinal and circumferential interacting corrosion defect spacing), and the internal pressure loading respectively. This affirms similar probability distribution models identified by Refs. [3,21,22] for the reliability assessment of corroded pipelines.

Additionally, the design of experiments employed interpolation and regression approaches such as Kriging design, central composite design and optimal space-filling design to generate the design and response points over the sampling space. The Kriging design provided the best design space coverage and response surface fit by producing better goodness of fit estimates than the other approaches. A further examination of the design of experiments to determine the relative degree of influence of the design variables on the true burst pressure response was conducted using a sample-based sensitivity. The results, for example, as shown in Fig. 18 highlighted the plastic failure of the corroded pipe by the noticeable influence from the ultimate tensile strength and insignificant contribution from the tensile yield strength. Also, the burst pressure heavily depends on the maximum corrosion cluster defect depth, pipeline external diameter, wall thickness, effective corrosion cluster defect length, and the longitudinal and circumferential interacting corrosion defect spacing. However, the relative influence from the minimum corrosion cluster defect depth, the effective corrosion cluster defect width, the internal pressure, and tensile yield strength were insignificant and not considered in the surrogate modelling stage based on a Cotter index limit of 0.025.

To reduce the computational cost of numerical modelling, a polynomial chaos-Kriging that utilizes interpolation and regression methods to capture the global and local design space was employed to generate the design and response surface. It was observed that polynomial chaos-Kriging produced the best fit by yielding a leave out error of 0.40, less than the leave out errors of 2.22 and 6.94 produced by the polynomial Kriging and Sector Vector Regression method, respectively. A surrogate-based active learning reliability without a closed form solution limit states was employed to determine the probability of failure of the corroded pipeline with interacting features. The likelihood of failure estimates by all reliability methodologies taken into consideration were found to be about 10^{-7}. However, the active learning reliability, on the other hand, approaches a reliable and narrow confidence interval for the probability of failure between 1.5473 $\times 10^{-7}$ to 2.4105 $\times 10^{-7}$ while the other approaches result in a wider interval. Additionally, the active learning reliability approach has a lower computational cost than simulation-based methods. The consideration of corrosion growth rate together with related uncertainties is beyond the scope of the present work and will be investigated in the next stage of this research.

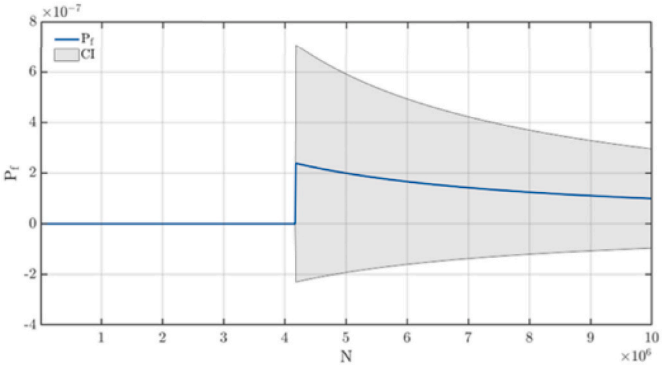

Fig. 22. Importance sampling reliability plot.

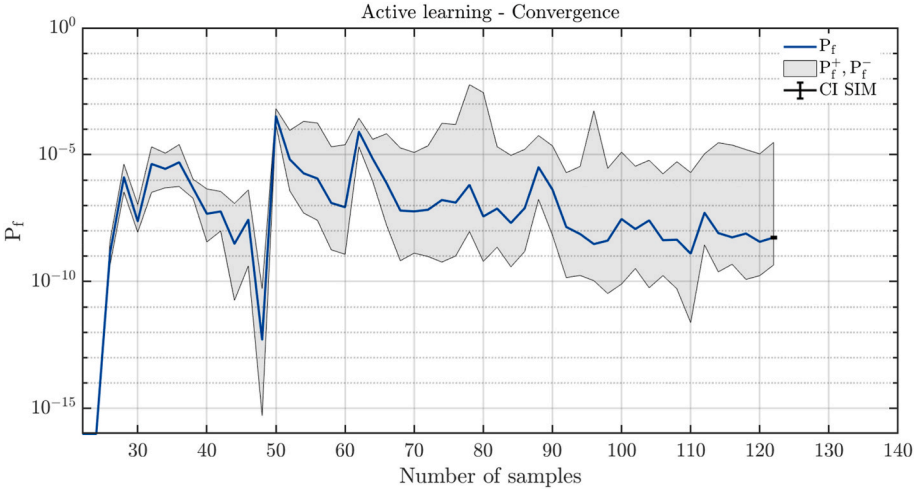

Fig. 21. Surrogate-based active learning reliability plot.

Declaration of competing interest

The authors declare the following financial interests/personal relationships which may be considered as potential competing interests: Abraham Mensah reports financial support was provided by Ghana National Petroleum Corporation (GNPC) Foundation - PhD Scholarship. Abraham Mensah reports a relationship with Ghana National Gas Company (GNGC), Accra, Ghana that includes: employment.

Data availability

The authors do not have permission to share data.

Acknowledgments

The first author would like to thank the Ghana National Petroleum Corporation (GNPC) Foundation for funding the PhD studies at the University of Aberdeen, United Kingdom. The first author also acknowledges the research support from Net Zero Technology Centre and University of Aberdeen through their partnership in the UK National Decommissioning Centre.

References

[1] H.A. Kishawy, H.A. Gabbar, Review of pipeline integrity management practices, Int. J. Pres. Ves. Pip. 87 (7) (Jul. 2010) 373–380, https://doi.org/10.1016/j.ijpvp.2010.04.003.

[2] A. Valor, F. Caleyo, J.M. Hallen, J.C. Velázquez, Reliability assessment of buried pipelines based on different corrosion rate models, Corrosion Sci. 66 (Jan. 2013) 78–87, https://doi.org/10.1016/j.corsci.2012.09.005.

[3] A.P. Teixeira, C. Guedes Soares, T.A. Netto, S.F. Estefen, Reliability of pipelines with corrosion defects, Int. J. Pres. Ves. Pip. 85 (4) (Apr. 2008) 228–237, https://doi.org/10.1016/j.ijpvp.2007.09.002.

[4] U. Bhardwaj, A.P. Teixeira, C. Guedes Soares, M.S. Azad, W. Punurai, P. Asavadorndeja, Reliability assessment of thick high strength pipelines with corrosion defects, Int. J. Pres. Ves. Pip. 177 (Nov. 2019), https://doi.org/10.1016/j.ijpvp.2019.103982.

[5] H. da C. Bisaggio, T.A. Netto, Predictive analyses of the integrity of corroded pipelines based on concepts of structural reliability and Bayesian inference, Mar. Struct. 41 (Apr. 2015) 180–199, https://doi.org/10.1016/j.marstruc.2015.02.003.

[6] Det Norske Veritas, Recommended Practice, DNV-RP-F101, Corroded Pipelines, 2004 [Online]. Available: http://www.dnv.com.

[7] R. Amaya-Gómez, M. Sánchez-Silva, E. Bastidas-Arteaga, F. Schoefs, F. Muñoz, Reliability assessments of corroded pipelines based on internal pressure – a review, in: Engineering Failure Analysis, vol. 98, Elsevier Ltd, Apr. 01, 2019, pp. 190–214, https://doi.org/10.1016/j.engfailanal.2019.01.064.

[8] M. Grubišić, J. Ivošević, A. Grubišić, Reliability analysis of reinforced concrete frame by Finite Element Method with implicit limit state functions, Buildings 9 (5) (2019), https://doi.org/10.3390/buildings9050119.

[9] C. Gong, D.M. Frangopol, Time-variant hull girder reliability considering spatial dependence of corrosion growth, geometric and material properties, Reliab. Eng. Syst. Saf. 193 (Jan. 2020), https://doi.org/10.1016/j.ress.2019.106612.

[10] British Standards Institution, European committee for standardization, in: Guide to Methods for Assessing the Acceptability of Flaws in Metallic Structures, British Standards Institution, 2005.

[11] A.C. Benjamin, J.L.F. Freire, R.D. Vieira, Part 6: analysis of pipeline containing interacting corrosion defects, Exp. Tech. 31 (3) (May 2007) 74–82, https://doi.org/10.1111/j.1747-1567.2007.00190.x.

[12] A.C. Benjamin, J.L.F. Freire, R.D. Vieira, D.J.S. Cunha, Interaction of corrosion defects in pipelines – Part 2: MTI JIP database of corroded pipe tests, Int. J. Pres. Ves. Pip. 145 (Sep. 2016) 41–59, https://doi.org/10.1016/j.ijpvp.2016.06.006.

[13] R.E. Melchers, New insights from probabilistic modelling of corrosion in structural reliability analysis, Struct. Saf. 88 (Jan. 2021), https://doi.org/10.1016/j.strusafe.2020.102034.

[14] De Andrade EQ and Benjamin AC, "Finite element modeling of the failure behavior of pipelines containing interacting corrosion defects," in Proceeding of the ASME 25th International Conference on Offshore Mechanic and Arctic Engineering, Hamburg, Germany,.

[15] A.N.S.Y.S. Manual, Theory reference for the mechanical APDL and mechanical applications, Release 12 (0) (2009).

[16] A. Mensah, S. Sriramula, Estimation of burst pressure of pipelines with interacting corrosion clusters based on machine learning models, J. Loss Prev. Process. Ind. (Sep. 2023), 105176, https://doi.org/10.1016/j.jlp.2023.105176.

[17] W.Z. Xu, C.B. Li, J. Choung, J.M. Lee, Corroded pipeline failure analysis using artificial neural network scheme, Adv. Eng. Software 112 (Oct. 2017) 255–266, https://doi.org/10.1016/j.advengsoft.2017.05.006.

[18] DesignXplorer User's Guide, 2022 [Online]. Available: http://www.ansys.com.

[19] R.C.C. Silva, J.N.C. Guerreiro, A.F.D. Loula, A study of pipe interacting corrosion defects using the FEM and neural networks, Adv. Eng. Software 38 (11–12) (2007) 868–875, https://doi.org/10.1016/j.advengsoft.2006.08.047.

[20] S. Reh, J.D. Beley, S. Mukherjee, E.H. Khor, Probabilistic finite element analysis using ANSYS, Struct. Saf. 28 (1–2) (Jan. 2006) 17–43, https://doi.org/10.1016/j.strusafe.2005.03.010.

[21] U. Bhardwaj, A.P. Teixeira, C. Guedes Soares, Uncertainty quantification of burst pressure models of corroded pipelines, Int. J. Pres. Ves. Pip. 188 (Dec) (2020), https://doi.org/10.1016/j.ijpvp.2020.104208.

[22] I.A. Chaves, R.E. Melchers, Extreme value analysis for assessing structural reliability of welded offshore steel structures, Struct. Saf. 50 (2014) 9–15, https://doi.org/10.1016/j.strusafe.2014.03.007.